Research Article

Graphene/Sulfur@Graphene Composite Structure Material for a Lithium-Sulfur Battery Cathode

Zengren Tao,[1] **Jianrong Xiao** ![ID],[1,2] **Zhiyun Yang,**[1] **and Heng Wang** ![ID][1]

[1]*College of Science, Guilin University of Technology, Guilin, China*
[2]*Guangxi Key Laboratory of Electrochemical and Magnetochemical Functional Materials, Guilin University of Technology, Guilin, China*

Correspondence should be addressed to Jianrong Xiao; xjr@glut.edu.cn and Heng Wang; wangh@glut.edu.cn

Graphene/sulfur@graphene composite structure as a cathode material is synthesized with a facile method. Graphene can provide a more efficient conductive network for sulfur and improve the coulombic efficiency of the battery. On the other hand, it may also show the anchoring effect on sulfur, which reduces the loss of sulfur and improves the cycling performance of the battery. Due to the unique structure, the initial discharge capacity of a battery assembled with this structure could reach $1036 \, \text{mAh g}^{-1}$ at 0.1 C, and its reversible capacity of $619 \, \text{mAh g}^{-1}$ was retained after 200 cycles with a low fading rate of 0.2% per cycle. The battery could hold a discharge capacity of $501 \, \text{mAh g}^{-1}$ after 200 cycles at 0.5 C. Thus, the electrochemical performance improved because of the reduction of sulfur loss through polysulfide accumulation at the cathode.

1. Introduction

High-energy-density rechargeable batteries are essential for various applications, such as portable electronic devices and grid-scale renewable energy storage, especially electric vehicles [1]. In various candidate electrochemical energy storage systems, lithium-sulfur (Li-S) batteries have various advantages, such as high theoretical specific capacity ($1675 \, \text{mAh g}^{-1}$), low operating voltage (2.2 V), abundant S storage, low cost, and environment-friendly property, thereby showing potential for commercial applications [2–4].

However, various problems, such as low conductivity of S and lithium sulfide, hinder the commercialization of Li-S batteries, the utilization of active substances, and the rate performance of batteries. Lithium polysulfide (Li_2S_n), an intermediate product generated during charge and discharge, can be dissolved in electrolytes and shuttled between positive and negative electrodes, thereby inducing the rapid fading of capacity. The volume of S expands up to 80% during discharge, causing the positive electrode to be powdered and the batteries to fail [1, 3–7].

To alleviate these problems and improve the electrochemical performance of Li-S batteries, researchers extensively investigated the cathodes, anodes, electrolytes, and separators of Li-S batteries. The conductivity of electrodes can be effectively enhanced by uniformly loading S on a conductive carrier [8–11], and the volume expansion of S can be effectively alleviated by designing suitable pore structures or using flexible carriers [12–14]. In restraining the shuttle effect of lithium polysulfide, studies can be divided into two categories. One category involves physical limiting effect, that is, by designing a carrier material with a large specific surface area and a rich pore structure to adsorb lithium polysulfide [15, 16]. The other category is chemisorption, which limits the dissolution and diffusion of lithium polysulfide between polar carrier materials and lithium polysulfide [17]. Short-chain S molecules and compounds forming S bonds have been used to avoid the shuttle effect [18, 19]. In studies on cathode materials, especially structural designs, many interesting structures, such as coaxial carbon nanotube structure [20–23], dual-core shell structure [24–26], and plane hierarchical structure [11, 27–29], have been proposed, and the

electrochemical performance of Li-S batteries has been effectively improved.

The preparation of plane hierarchical structures is relatively simple, and the electrochemical performance of batteries with these structures as cathodes is enhanced. These structures exhibit many excellent properties. First, they can prevent active materials from escaping from cathodes, reduce the loss of active materials, and improve cycle stability [27]. Second, these structures can provide the conductivity and coulombic efficiency of the battery by creating an effective conductive network [30]. Third, these structures can alleviate volume change because more spaces are available for active substances [12, 13]. Therefore, the electrochemical performance of Li-S batteries can be improved by designing a hierarchical cathode mixture.

Graphene (G), a 2D monolayer carbon structure, is the thinnest material in the world. Its electron mobility is higher than 15,000 cm^2/(V·s) at room temperature and higher than those of carbon nanotubes and silicon crystals. Its resistivity (10^{-6} Ω·cm) is lower than those of copper and silver, and its strength is 100 times higher than that of steel [31, 32]. It can effectively improve the conductivity of S-based electrodes, limit the diffusion of soluble polysulfide, and alleviate the volume expansion of electrodes.

In this study, graphene/sulfur@graphene (G/S-G) composite structure materials were prepared by using G and S. A simple preparation method was proposed to fabricate cathode materials. Hierarchical cathodes displayed good cyclability and alleviated volume expansion. They were investigated by analyzing their activation process and excellent polysulfide retention attributed to the hierarchical electrode structure.

2. Experimental Section

2.1. Preparation of G/S Active Material. S and G (Nanjing Xian Feng Nanometer Co. Ltd., China) were placed in an agate mortar with a mass ratio of $7 : 3$, ground for 1 h, and transferred to a polytetrafluoroethylene reaction vessel. Then, we keep the vessel static and open it in an argon-filled glove box for 45 min to exclude the air to avoid the oxidation of the S during the reaction. The reaction vessel was heated at 155°C for 12 h. At this temperature, the melted S could easily penetrate the reticular structure of G. Finally, the G/S composite was obtained after the specimen was cooled to room temperature.

2.2. Preparation of Composite Structure. The working electrodes were prepared from the G/S composite, Super P, and the PVDF binder in NMP with a mass ratio of $8 : 1 : 1$. The cathode mixture paste was dropped onto an aluminum foil. Three active materials were prepared: (a) a S monolayer, (b) a G/S monolayer, and (c) a G/S monolayer coated with G (graphene/sulfur@graphene (G/S-G) composite materials). These mixtures were dried in an oven at 60°C for 12 h. The cathode was punched into a disk with a diameter of 14 mm for assembling.

2.3. Cell Assembly. CR-2025-type button cells were used to test the electrochemical performance of the S cathode. They were assembled in an argon-filled glove box by using the three cathode mixtures. Li was used as a counter electrode, and 1 M Li TFSI/DME+DOL (1 : 1, V/V) containing 1 wt% LiNO$_3$ was used as an electrolyte. The battery is assembled from top to bottom according to Li anodes, electrolytes, separators (polypropylene, Celgard, 2400), and cathodes (G/S-G, G/S, and S). Pouch cells were sealed with a soft aluminum packaging film. The assembled coin and pouch cells were allowed to rest for 12 h at 25°C before electrochemical measurements were carried out.

2.4. Material Characterization. A field emission scanning electron microscope (SEM, Hitachi S-4800) was used to characterize the morphology of the cathode before and after 200 cycles. An energy-dispersive spectrometer (EDS) was utilized to identify the distribution of the elements on the surface of the G/S-G cathode. An X-ray diffractometer (XRD, X'Pert PRO) was used to characterize the phase structure and crystallinity of the G/S-G, G/S monolayer, and S monolayer.

2.5. Electrochemical Measurement. Cyclic voltammetry (CV) and electrochemical impedance spectroscopy (EIS) were tested in an electrochemical workstation (CHI750E). Discharge and charge profiles and cyclability performance were evaluated under galvanostatic conditions between 1.5 and 2.8 V with a constant current density at 25°C. CV measurements were performed at a scan rate of 0.01 mVs^{-1} in the voltage range of 1.5–3.0 V at 25°C. EIS tests were performed at a frequency range of 0.01–100 kHz with a perturbation amplitude of 5 mV at 25°C.

3. Results and Discussion

3.1. Configuration and Morphology. Figure 1 illustrates the schematic of the designed G/S monolayer and G/S-G and the changes in the G/S-G cathode after cycling. The G/S cathode was synthesized by heating the mixture of G and S at high temperature (Figure 1(a)). S is covered by G layers and protected to a certain extent, but many S losses still occurred during the cycle. G/S-G could be obtained by coating a layer of G on G/S (Figure 1(b)). S was further protected by adding a layer of G, which could provide more attachment points for active substances and to a certain extent alleviate the shuttle effect. Figure 1(c) shows the schematic of G/S-G before and after the cycle. As the reaction proceeded, S and Li$_2$S$_n$ were constantly intercepted and attached to G. After cycles, the volume of the cathode increased. However, G could effectively improve the conductivity of S because G had a honeycomb crystal structure, good conductivity, and high chemical stability; thereby, it can improve the electrochemical reaction efficiency of active substances and limit the diffusion of soluble polysulfide and effectively alleviate the volumetric expansion effect of the electrode.

Figure 2 shows the XRD patterns of the S, G/S, and G/S-G samples. The single-mass S peak was strong and sharp, and obvious diffraction peaks appeared in the whole scanning range, suggesting that the material has a strong crystal structure. The main diffraction peaks were located at 23.48° and
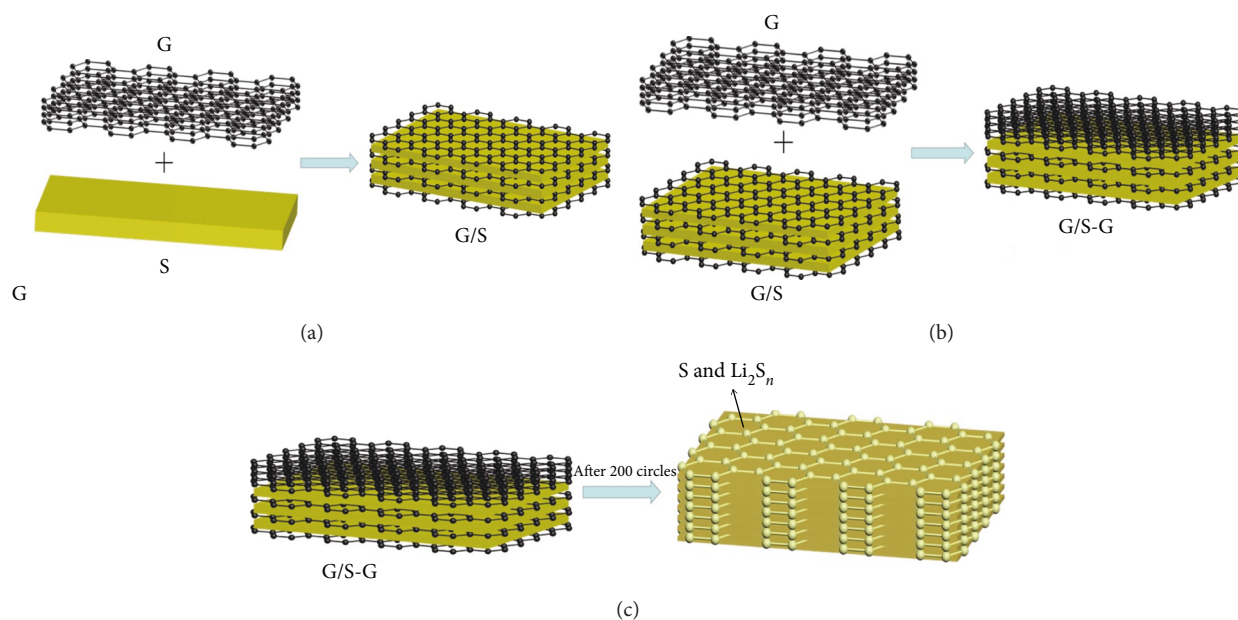
FIGURE 1: Cathode configuration diagram of the preparation of (a) G/S and (b) G/S-G and (c) the structural changes after the cycles of G/S-G.
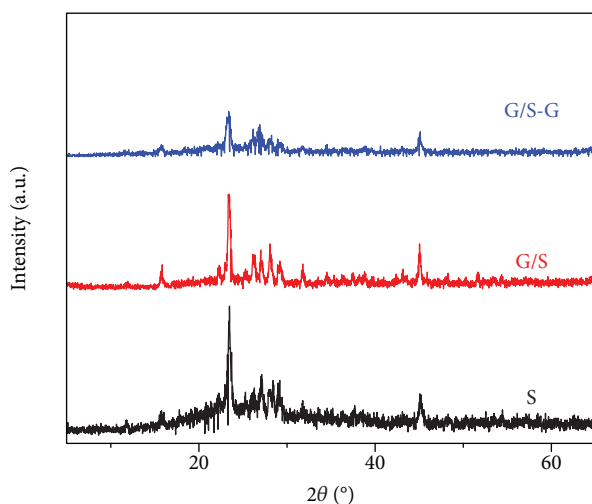

FIGURE 2: XRD patterns of G/S-G, G/S, and S.

27.12°, which originated from the skew square-type diffraction and a typical S_8 structure [9, 33]. The G reflections were mainly located between 20° and 30°, indicating an amorphous state. For the G/S-G and G/S samples, the diffraction peaks at 20°–30° had different intensities. The results implied that the crystallinity and amorphous states of sublimated S were found in the composites. The differences in the relative intensity of the main reflection peak of the three samples could be due to the different S contents in the sample. The diffraction peaks of the G/S cathode were evident because of the high S content on the surface layer. For example, the S content in G/S was 70%. Conversely, these peaks were weaker than those on the S monolayer. The diffraction peaks of G/S-G cathode materials were much weaker because S had the lowest content on the G surface layer, so the entire S was covered by G, and the amorphous structure of the materials was enhanced.

The SEM image of the surface of the positive pole of G/S-G before and after 200 cycles is shown in Figure 3. Before the cycle, the G/S-G surface was covered with some granular matters, specifically PVDF and Super P, and G could be located below the granular material. In Figures 3(a) and 3(b), G was uniformly distributed on the surface, effectively providing the conductive path for S, blocking the diffusion of polysulfide, and suppressing the shuttle effect.

The SEM image of the G/S-G cathode after 200 cycles at 0.1 C is illustrated in Figures 3(c) and 3(d). Before cycling occurred, PVDF and Super P were attached to the G surface, which was relatively smooth. PVDF and Super P disappeared, and the G surface was thickened by a cloud-like substance, which could be S and intermediate products, such as lithium polysulfide [34, 35], and was obstructed by G. The EDS of the surface of the G/S-G cathode before and after the cycle is shown in Figure 4(a). The signal of C was considerably stronger than that of S because S was covered by G in the composite structure. The signal of S was enhanced, whereas the signal of C was weakened because of polysulfide accumulation on the surface after the cycle. The signals of three elements, namely, O, F, and C, were enhanced and uniformly dispersed.

The SEM image of the cross section of the G/S-G cathode before and after the cycle is shown in Figure 5. The G/S-G structure could be seen in the hierarchical cathode before the cycle. However, this structure could not be easily distinguished after 200 cycles at 0.1 C because of the continuous diffusion of polysulfide to the surface layer and the uniform diffusion of the active substance throughout the cathode during the battery cycle. In addition, the thickness of the cathode mixture increased from 11.7 μm to 18 μm during the cycle, indicating a remarkable volumetric expansion within the measurement error. However, further polysulfide migration could be hindered by the G layer to reduce the loss of the active materials because of the hierarchical structure, and volume expansion could be alleviated.
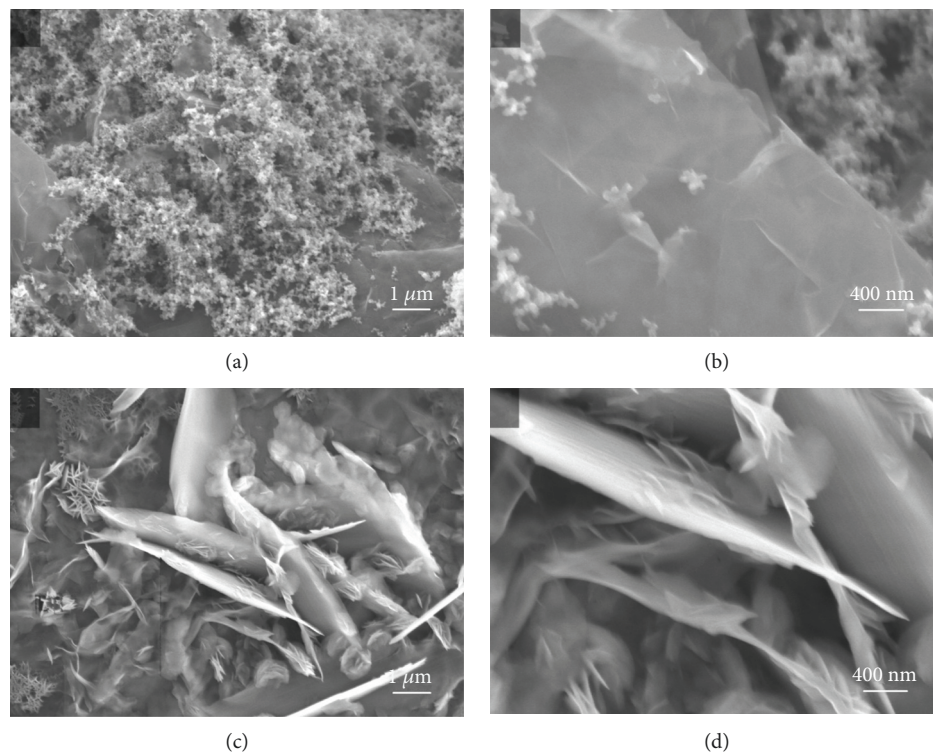
(a)

(b)

(c)

(d)

Figure 3: High-magnification SEM images of the G/S-G cathode (a, b) before and (c, d) after 200 cycles at 0.1 C.
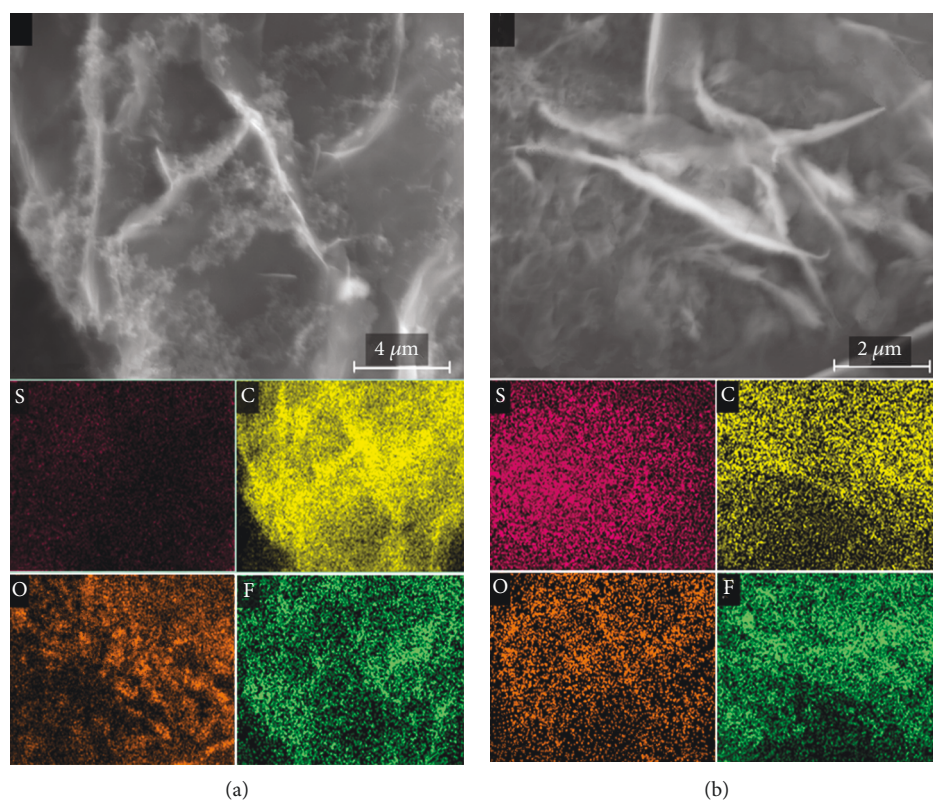

(a)

(b)

Figure 4: SEM images and elemental mapping of the G/S-G cathode (a) before and (b) after 200 cycles at 0.1 C.
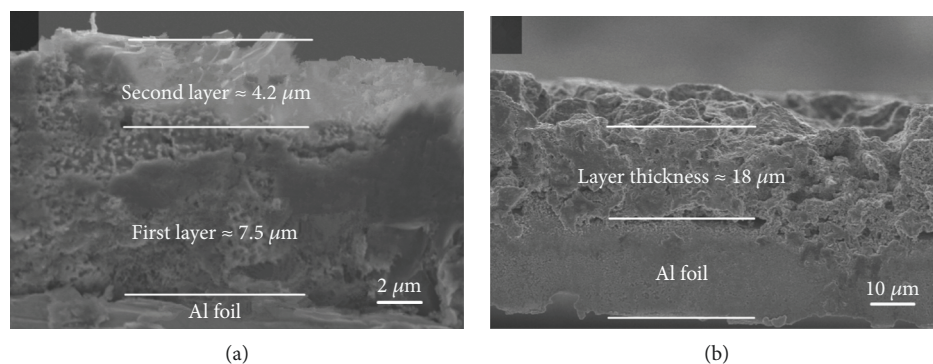
FIGURE 5: SEM images of the G/S-G cathode cross section (a) before and (b) after 200 cycles at 0.1 C.
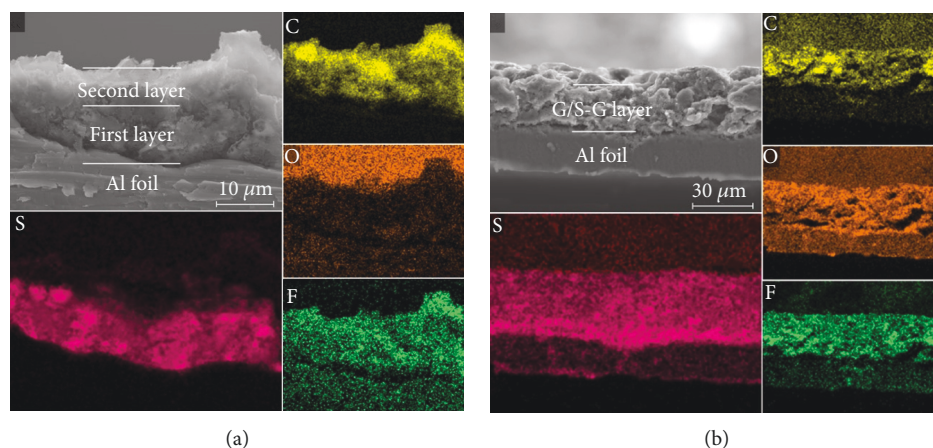

FIGURE 6: SEM images and elemental mapping of the G/S-G cathode cross section (a) before and (b) after 200 cycles at 0.1 C.

The EDS of the cross section of the layered cathode is presented in Figure 6. S was mostly located in the first layer before the cycle. The S content increased and was uniformly distributed in the first layer after 200 cycles. S-containing species started to diffuse from the active material layers and were obstructed by the G of the upper layer as a result of the stabilized polysulfide migration.

3.2. Electrochemical Stability.

To further determine whether the electrochemical performance of the Li-S battery with this hierarchical structure as the cathode could be improved effectively, we measured the cycling performances at different C rates. With the preferable electrochemical utilization and cycle stability, the hierarchical cathode batteries could attain high discharge capacity and long-term cyclability for 200 cycles at various cycling rates (Figure 7). The coulombic efficiency of G/S-G was greater than 95% (Figure 7(a)), indicating that the structure cathode battery had a high reversible capacity. In Figures 7(b) and 7(c), the initial discharge capacities of G/S-G and G/S at 0.1 C reached 1016 and 819 mAh g^{-1}, respectively. At 0.2 C after 200 cycles, their discharge capacities were 887 and 787 mAh g^{-1}, respectively. Their corresponding discharge capacities were 793 and 686 mAh g^{-1} at 0.1 C and 590 and 521 mAh g^{-1} at 0.2 C, respectively. The capacity fading of the G/S-G and G/S was about 30% after 200 cycles at 0.2C, and it was higher than that of the pure S (about 75% after 100 cycles at 0.2 C). The

coulombic efficiencies of the batteries were higher than 95%. The discharge capacity of the batteries remarkably improved compared with that of the original S monolayer structure, especially the G/S-G structure, because there is an extra G layer; polysulfide diffusion was hindered by the G upper layer during the charge/discharge process, and it provides more attachment points for sulfur and improves the efficiency of ion transport. The capacity of the first discharge of G/S-G reached 775 mAh g^{-1} at 0.5 C, and its favorable capacity of 502 mAh g^{-1} was retained after 200 cycles (Figure 7(d)).

Figures 7(e) and 7(f) show the charge and discharge curves of the batteries with the G/S and G/S-G cathodes at the given C rates. The voltage plateau gap was 0.566 V for the sulfur cathode with G/S at 0.2 C and 0.589 V at 0.5 C. The use of G/S-G in the sulfur cathode decreased the voltage plateau gap to 0.303 V at 0.2 C and to 0.376 V at 0.5 C. The decreased voltage gap indicates the decreased resistance and simple electrode kinetics of the G/S-G cathode [36].

Figure 8(a) shows the cycling performance of the batteries (G/S, G/S-G, and S) at different C rates (0.1 C→0.2 C→0.3 C→0.5 C→0.1 C→0.5 C→0.3 C→0.2 C). The initial discharge capacity of the cell with the G/S-G hierarchical cathode reached 1067 mAh g^{-1}. Although the capacity of the battery declined rapidly in the first five cycles, the capacity of the battery began to stabilize as the current density increased. The capacity of the battery slowly decreased from
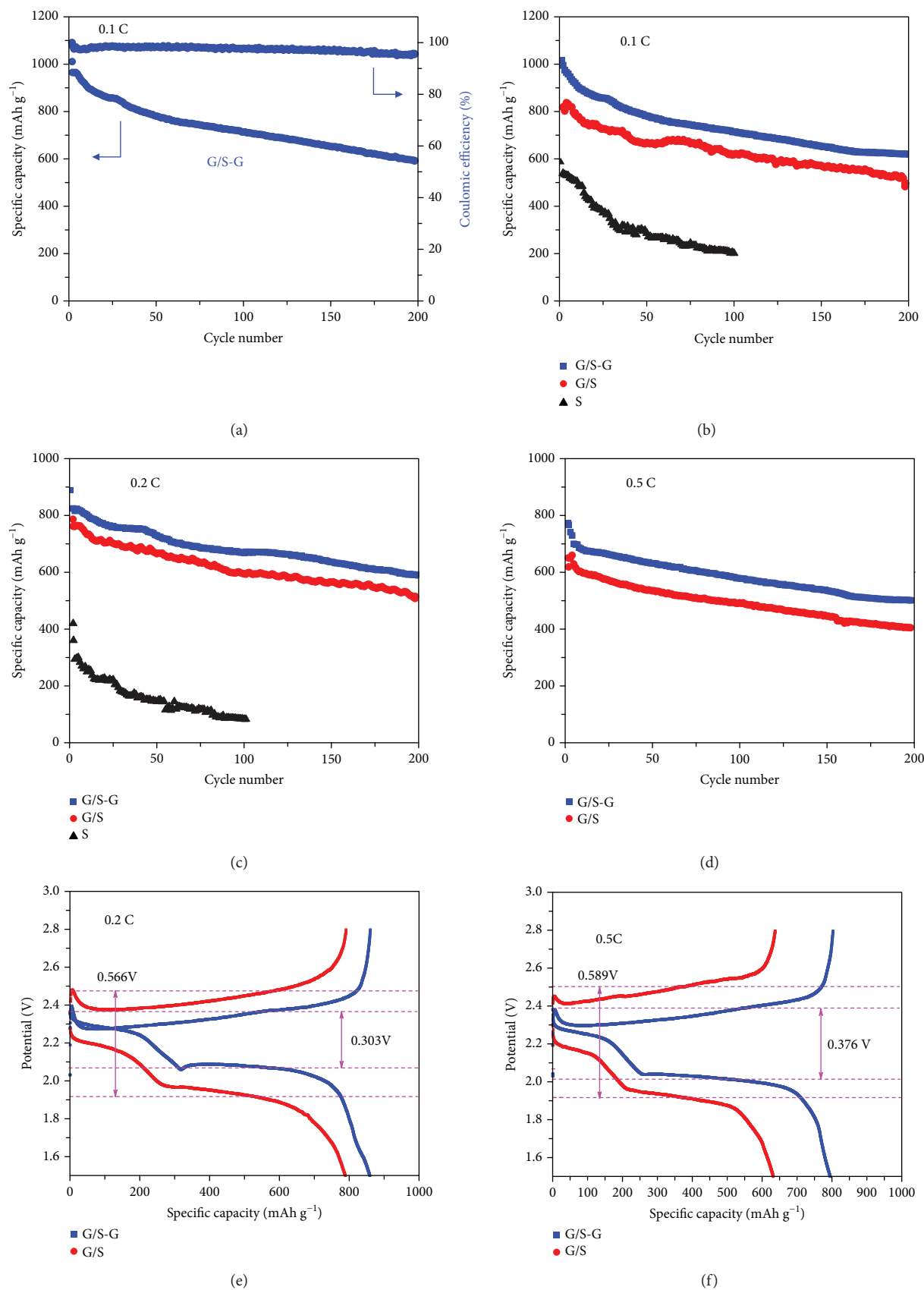
(a)

(b)

(c)

(d)

(e)

(f)

FIGURE 7: Cycling performance of Li-S cells with G/S-G, G/S monolayer, and S monolayer cathodes at (a) 0.1, (b) 0.1, (c) 0.2, and (d) 0.5 C. (e, f) Galvanostatic discharge-charge curves at different C rates in the 1.5–2.8 V voltage window.
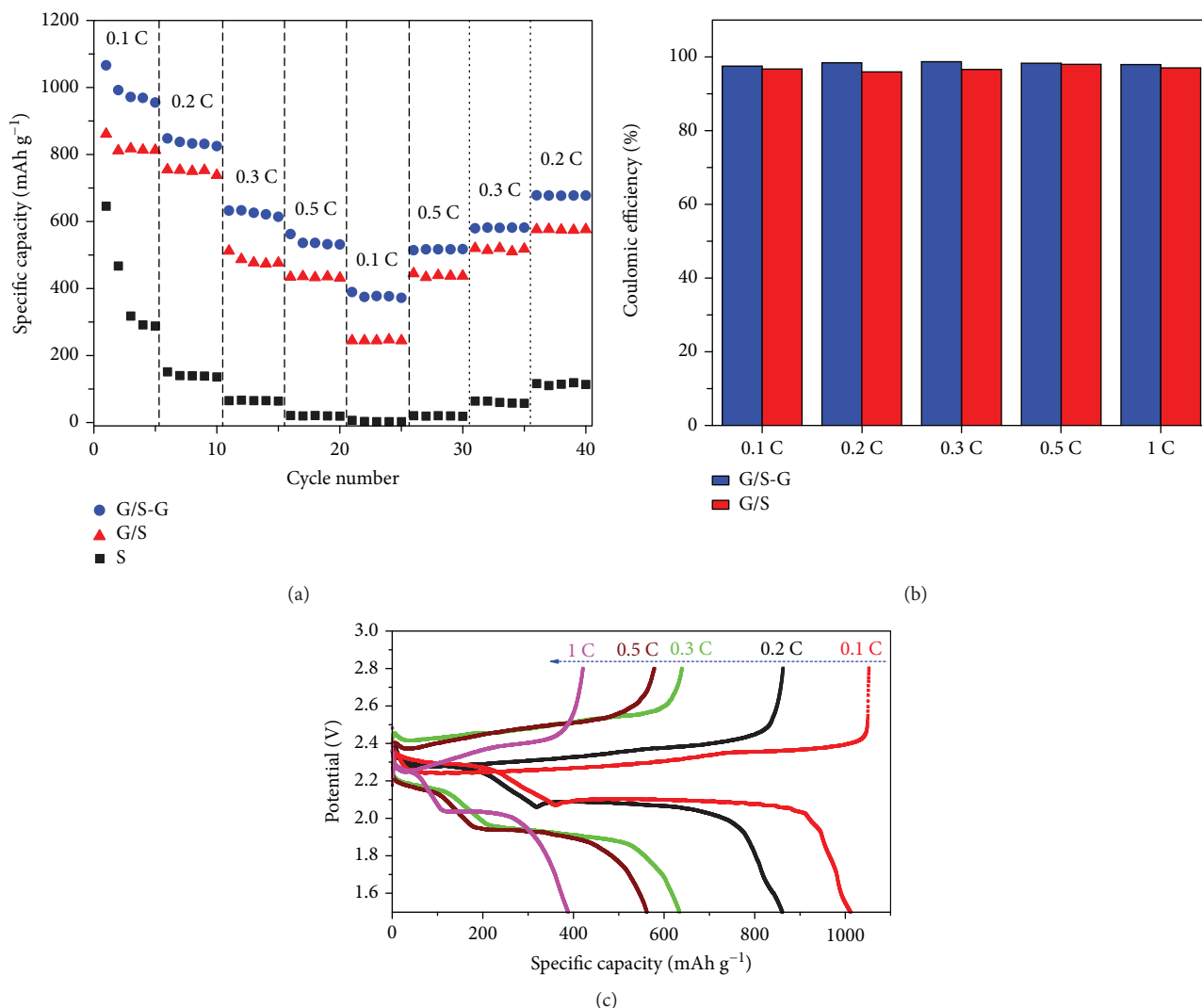
(a)

(b)

(c)

Figure 8: (a) Rate performance of G/S-G and G/S and S monolayers, (b) average coulombic efficiency of G/S-G and G/S at different rates, and (c) initial discharge/charge curves of the G/S-G cathode at various C rates from 0.1 C to 1 C.

955 mAh g^{-1} at 0.1 C to 848, 633, and 563 mAh g^{-1} at 0.2, 0.3, and 0.5 C, respectively. When the current rate returned to 0.1 C, the capacity of the G/S-G battery was higher than that of the two other batteries, indicating that the planar double-layer structure could limit polysulfide diffusion. The electrochemical performance of the batteries with the G composite (G/S/-G and G/S) was better than that with the S monolayer cell because of the excellent conductivity and the effect of S aggregation. Both batteries with the G composite maintained a high coulombic efficiency even at a high rate (Figure 7(b)). Figure 8(c) shows the charge/discharge profiles of G/S-G at various rates. The characteristic hierarchical structure of G/S-G could be clearly identified at 0.1 C, presenting a long charge/discharge plateau, which indicated low polarization. S can be fully transferred to Li$_2$S$_2$/Li$_2$S, thereby enhancing the utilization of active materials [36, 37].

Figure 9(a) shows the typical CVs at a scan rate of 0.1 mVs^{-1} with a potential range of 1.5–3 V. Two cathodic peaks were observed at 2.0 and 2.3 V, which were due to insoluble Li$_2$S$_2$/Li$_2$S and high-order S$_n$ formation ($4 \leq n \leq 8$),

respectively. In the subsequent anodic scan, two oxidation peaks corresponding to the oxidation of insoluble Li$_2$S$_2$/Li$_2$S to soluble polysulfides were observed [37–39]. The CVs of the G/S-G battery showed that the current density of the redox peaks was large and stable, indicating low polarization, good reversibility, and excellent cycling stability. Therefore, the electrochemical stability of the Li-S battery could be improved by designing the hierarchical structure cathode because of the polysulfide accumulation effect of G. Figure 9(b) illustrates the charge/discharge curves of G/S-G batteries within the given cycles at 0.1 C. The high-voltage discharge plateau at 2.3 V corresponded to the reduction of S, leading to soluble polysulfide formation.

To further understand the contribution of the designed plane hierarchical structure to the electrochemical performance, we performed EIS (Figure 10). R_1 in the illustrations denotes the resistance of the electrolyte, R_2 corresponds to the charge transfer resistance of the battery, CPE$_1$ refers to the constant phase element, and W_1 represents the Walburg diffusion impedance. The electrochemical impedance curves
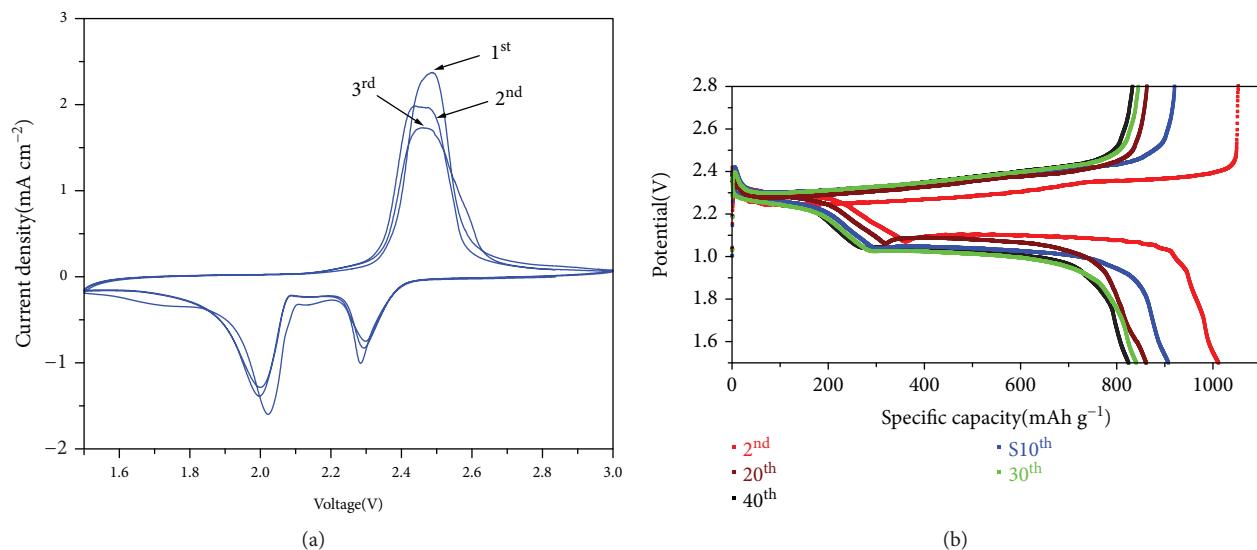
FIGURE 9: (a) CV curves at a scan rate of 0.1 mV s^{-1} and (b) the 2nd to the 40th discharge/charge curves of the G/S-G cathode at 0.1 C between 1.5 and 2.8 V.
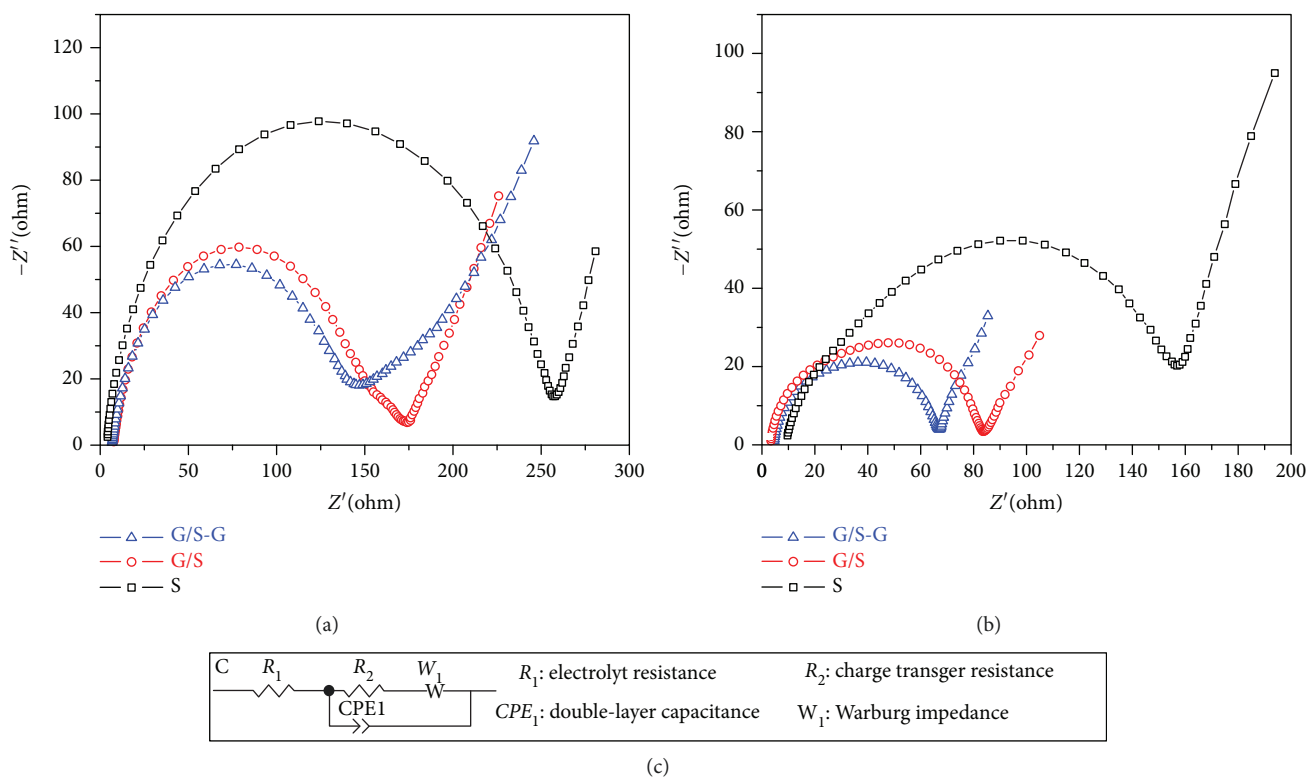

FIGURE 10: EIS of the cells with G/S-G, G/S, and S monolayer cathodes (a) before and (b) after 200 cycles at 0.1 C. (c) Equivalent circuit used to fit the impedance spectra.

were composed of two medium- and high-frequency semicircles corresponding to the charge transfer resistance and a low-frequency sloping line corresponding to the Warburg impedance. The ohmic resistance of the Li-S battery could be derived from the intercept at the Z' axis [40, 41]. The diameters of the semicircles provided the overall interface resistance of the battery. Several features are given in Table 1 and Figures 10(a) and 10(b). The battery with the G/S-G cathode showed the smallest charge transfer resistance before and after cycling. The charge transfer resistance decreased after cycling possibly because of the uniform distribution of active S.

Table 1: Impedance parameters of Li-S coin cells with S, G/S, and G/S-G cathodes before discharge and after cycles.

Cathode	R_1 (Ω)	R_2 (Ω)
S (before discharge)	14.67	257.00
G/S (before discharge)	6.78	174.00
G/S-G (before discharge)	18.05	147.00
S (after the 100th cycle)	20.24	157.00
G/S (after the 200th cycle)	3.49	83.60
G/S-G (after the 200th cycle)	3.99	67.20

4. Conclusions

In this study, G/S-G composite structure cathode materials were synthesized using a low-cost method, and their application in Li-S batteries was studied. A cathode with this structure could limit the diffusion of soluble polysulfide, reduce the volume expansion of electrodes, and enhance the electrochemical stability of Li-S batteries. The attenuation rate of the capacity of the battery was 0.2%, and stable cyclability of more than 200 times was achieved. Polysulfide migration was analyzed through cross-sectional SEM and elemental analysis. The improved electrochemical performance could be ascribed to the special hierarchical structure, which could restrain the dissolution of polysulfides by the film-forming property of G. Therefore, cathodes with a hierarchical structure showed potential for applications in Li-S batteries with stable cyclability.

Data Availability

The data used to support the findings of this study are available from the corresponding author upon request.

Conflicts of Interest

The authors declare that there is no conflict of interests regarding the publication of this paper.
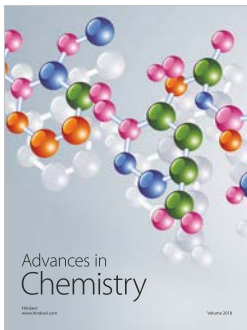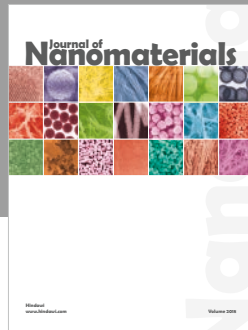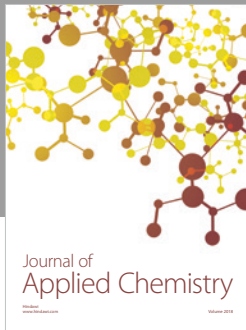
Acknowledgments

References

[1] A. Manthiram, S. H. Chung, and C. Zu, "Lithium-sulfur batteries: progress and prospects," *Advanced Materials*, vol. 27, no. 12, pp. 1980–2006, 2015.

[2] R. Song, R. Fang, L. Wen, Y. Shi, S. Wang, and F. Li, "A trilayer separator with dual function for high performance lithium–sulfur batteries," *Journal of Power Sources*, vol. 301, pp. 179–186, 2016.

[3] P. G. Bruce, S. A. Freunberger, L. J. Hardwick, and J. M. Tarascon, "Li–O_2 and Li–S batteries with high energy storage," *Nature Materials*, vol. 11, no. 2, p. 172, 2012.

[4] R. Fang, S. Zhao, Z. Sun, D. W. Wang, H. M. Cheng, and F. Li, "More reliable lithium-sulfur batteries: status, solutions and prospects," *Advanced Materials*, vol. 29, no. 48, article 1606823, 2017.

[5] C. Barchasz, F. Molton, C. Duboc, J. C. Leprêtre, S. Patoux, and F. Alloin, "Lithium/sulfur cell discharge mechanism: an original approach for intermediate species identification," *Analytical Chemistry*, vol. 84, no. 9, pp. 3973–3980, 2012.

[6] S. E. Cheon, S. S. Choi, J. S. Han, Y. S. Choi, B. H. Jung, and H. S. Lim, "Capacity fading mechanisms on cycling a high-capacity secondary sulfur cathode," *Journal of the Electrochemical Society*, vol. 151, no. 12, pp. A2067–A2073, 2004.

[7] Y. V. Mikhaylik and J. R. Akridge, "Polysulfide shuttle study in the Li/S battery system," *Journal of the Electrochemical Society*, vol. 151, no. 11, pp. A1969–A1976, 2004.

[8] X. Ji, K. T. Lee, and L. F. Nazar, "A highly ordered nanostructured carbon–sulphur cathode for lithium–sulphur batteries," *Nature Materials*, vol. 8, no. 6, pp. 500–506, 2009.

[9] J. Xiao, H. Wang, X. Li, Z. Wang, J. Ma, and H. Zhao, "N-doped carbon nanotubes as cathode material in Li–S batteries," *Journal of Materials Science: Materials in Electronics*, vol. 26, no. 10, pp. 7895–7900, 2015.

[10] Y. Hou, J. Xiao, Y. Guo, M. Qi, A. Jiang, and Y. Li, "Gaseous-phase, silica-coated sulfur particles as a cathode material for high-performance lithium/sulfur batteries," *Journal of Materials Science: Materials in Electronics*, vol. 28, no. 12, pp. 8901–8907, 2017.

[11] B. Zhao, L. Zhang, Q. Zhang et al., "Rational design of nickel hydroxide-based nanocrystals on graphene for ultrafast energy storage," *Advanced Energy Materials*, vol. 8, no. 9, article 1702247, 2018.

[12] R. Fang, S. Zhao, S. Pei et al., "Toward more reliable lithium-sulfur batteries: an all-graphene cathode structure," *ACS Nano*, vol. 10, no. 9, pp. 8676–8682, 2016.

[13] D. W. Wang, G. Zhou, F. Li et al., "A microporous-mesoporous carbon with graphitic structure for a high-rate stable sulfur cathode in carbonate solvent-based Li-S batteries," *Physical Chemistry Chemical Physics*, vol. 14, no. 24, pp. 8703–8710, 2012.

[14] H. Wang, Y. Yang, Y. Liang et al., "Graphene-wrapped sulfur particles as a rechargeable lithium-sulfur battery cathode material with high capacity and cycling stability," *Nano Letters*, vol. 11, no. 7, pp. 2644–2647, 2011.

[15] Y. S. Su and A. Manthiram, "Lithium-sulphur batteries with a microporous carbon paper as a bifunctional interlayer," *Nature Communications*, vol. 3, no. 1, p. 1166, 2012.

[16] G. Zhou, L. Li, D. W. Wang et al., "A flexible sulfur-graphene-polypropylene separator integrated electrode for advanced Li-S batteries," *Advanced Materials*, vol. 27, no. 4, pp. 641–647, 2015.

[17] J. Liang, L. Yin, X. Tang et al., "Kinetically enhanced electrochemical redox of polysulfides on polymeric carbon nitrides for improved lithium-sulfur batteries," *ACS Applied Materials & Interfaces*, vol. 8, no. 38, pp. 25193–25201, 2016.

[18] B. Duan, W. Wang, A. Wang et al., "Carbyne polysulfide as a novel cathode material for lithium/sulfur batteries," *Journal of Materials Chemistry A*, vol. 1, no. 42, article 13261, 2013.

[19] N. Xu, T. Qian, X. Liu, J. Liu, Y. Chen, and C. Yan, "Greatly suppressed shuttle effect for improved lithium sulfur battery performance through short chain intermediates," *Nano Letters*, vol. 17, no. 1, pp. 538–543, 2017.

[20] X. Li, K. Ding, B. Gao et al., "Freestanding carbon encapsulated mesoporous vanadium nitride nanowires enable highly stable

sulfur cathodes for lithium-sulfur batteries," *Nano Energy*, vol. 40, pp. 655–662, 2017.

[21] S. Wang, B. Y. Guan, L. Yu, and X. W. D. Lou, "Rational design of three-layered TiO_2@carbon@MoS_2 hierarchical nanotubes for enhanced lithium storage," *Advanced Materials*, vol. 29, no. 37, article 1702724, 2017.

[22] J. Zhang, Y. Shi, Y. Ding, W. Zhang, and G. Yu, "In situ reactive synthesis of polypyrrole-MnO_2 coaxial nanotubes as sulfur hosts for high-performance lithium–sulfur battery," *Nano Letters*, vol. 16, no. 11, pp. 7276–7281, 2016.

[23] Q. Zhang, H. Chen, L. Luo et al., "Harnessing the concurrent reaction dynamics in active Si and Ge to achieve high performance lithium-ion batteries," *Energy & Environmental Science*, vol. 11, no. 3, pp. 669–681, 2018.

[24] S. Cheng, X. Xia, H. Liu, and Y. Chen, "Core-shell structured MoS_2@S spherical cathode with improved electrochemical performance for lithium-sulfur batteries," *Journal of Materials Science & Technology*, vol. 34, no. 10, pp. 1912–1918, 2018.

[25] X. Huang, K. Shi, J. Yang, G. Mao, and J. Chen, "MnO_2-GO double-shelled sulfur (S@MnO_2@GO) as a cathode for Li-S batteries with improved rate capability and cyclic performance," *Journal of Power Sources*, vol. 356, pp. 72–79, 2017.

[26] L. Ni, G. Zhao, G. Yang, G. Niu, M. Chen, and G. Diao, "Dual core–shell-structured S@C@MnO_2 nanocomposite for highly stable lithium–sulfur batteries," *ACS Applied Materials & Interfaces*, vol. 9, no. 40, pp. 34793–34803, 2017.

[27] S.-H. Chung, C.-H. Chang, and A. Manthiram, "Hierarchical sulfur electrodes as a testing platform for understanding the high-loading capability of Li-S batteries," *Journal of Power Sources*, vol. 334, pp. 179–190, 2016.

[28] G. Li, D. Luo, X. Wang et al., "Enhanced reversible sodium-ion intercalation by synergistic coupling of few-layered MoS_2 and S-doped graphene," *Advanced Functional Materials*, vol. 27, no. 40, article 1702562, 2017.

[29] Z. Tao, Z. Yang, Y. Guo, Y. Zeng, and J. Xiao, "Plane double-layer structure of AC@S cathode improves electrochemical performance for lithium-sulfur battery," *Frontiers in Chemistry*, vol. 6, p. 447, 2018.

[30] J. He, Y. Chen, W. Lv et al., "Three-dimensional hierarchical graphene-CNT@Se: a highly efficient freestanding cathode for Li–Se batteries," *ACS Energy Letters*, vol. 1, no. 1, pp. 16–20, 2016.

[31] S. V. Morozov, K. S. Novoselov, M. I. Katsnelson et al., "Giant intrinsic carrier mobilities in graphene and its bilayer," *Physical Review Letters*, vol. 100, no. 1, article 016602, 2008.

[32] A. K. Geim, "Graphene: status and prospects," *Science*, vol. 324, no. 5934, pp. 1530–1534, 2010.

[33] L. Yuan, X. Qiu, L. Chen, and W. Zhu, "New insight into the discharge process of sulfur cathode by electrochemical impedance spectroscopy," *Journal of Power Sources*, vol. 189, no. 1, pp. 127–132, 2009.

[34] Y. Guo, J. Xiao, Y. Hou, Z. Wang, and A. Jiang, "Carbon nanotube doped active carbon coated separator for enhanced electrochemical performance of lithium–sulfur batteries," *Journal of Materials Science: Materials in Electronics*, vol. 28, no. 23, pp. 17453–17460, 2017.

[35] Y. Guo, J. Xiao, Y. Hou, Y. Li, and A. Jiang, "Separators with active-carbon coating for advanced lithium–sulfur batteries," *International Journal of Electrochemical Science*, vol. 12, pp. 10850–10862, 2017.

[36] H. Lin, S. Zhang, T. Zhang et al., "Elucidating the catalytic activity of oxygen deficiency in the polysulfide conversion reactions of lithium-sulfur batteries," *Advanced Energy Materials*, vol. 8, no. 30, article 1801868, 2018.

[37] Z. Zhang, L. L. Kong, S. Liu, G. R. Li, and X. P. Gao, "A high-efficiency sulfur/carbon composite based on 3D graphene nanosheet@carbon nanotube matrix as cathode for lithium-sulfur battery," *Advanced Energy Materials*, vol. 7, no. 11, article 1602543, 2017.

[38] S. S. Zhang, "Liquid electrolyte lithium/sulfur battery: fundamental chemistry, problems, and solutions," *Journal of Power Sources*, vol. 231, no. 2, pp. 153–162, 2013.

[39] J. Zhu, Y. Ge, D. Kim et al., "A novel separator coated by carbon for achieving exceptional high performance lithium-sulfur batteries," *Nano Energy*, vol. 20, pp. 176–184, 2016.

[40] Z. Deng, Z. Zhang, Y. Lai, J. Liu, J. Li, and Y. Liu, "Electrochemical impedance spectroscopy study of a lithium/sulfur battery: modeling and analysis of capacity fading," *Journal of the Electrochemical Society*, vol. 160, no. 4, pp. A553–A558, 2013.

[41] V. S. Kolosnitsyn, E. V. Kuzmina, E. V. Karaseva, and S. E. Mochalov, "A study of the electrochemical processes in lithium–sulphur cells by impedance spectroscopy," *Journal of Power Sources*, vol. 196, no. 3, pp. 1478–1482, 2011.